Ligand-Field Dependence of the Excited State Dynamics of Hangman Bisporphyrin Dyad Complexes

Justin M. Hodgkiss, Alexander Krivokapić, and Daniel G. Nocera*

Department of Chemistry, 6-335, Massachusetts Institute of Technology, 77 Massachusetts Avenue, Cambridge, Massachusetts 02139-4307

Received: January 18, 2007; In Final Form: April 30, 2007

A new Hangman porphyrin architecture has been developed to interrogate the ligand-field dependence of photoinduced PCET versus excitation energy transfer and intersystem crossing in $PZn^{II}-PFe^{III}-OH$ dyads (P = porphyrin). In this design, a hanging carboxylic acid group establishes a hydrogen-bonding network to anchor the weak-field OH^- ligand in the distal site of the $PFe^{III}-OH$ acceptor, whereas the proximal site is left available to accept strong-field imidazole ligands. Thus, controlling the tertiary coordination environment gives access to the first synthetic example of a porphyrin dyad with a biologically relevant weak-field/strong-field configuration of axial ligands at the heme. Transient absorption spectroscopy has been employed to probe the fate of the initial PZn^{II}-based S_1 excited state, revealing rapid S_1 quenching for all dyads in the presence and absence of strong-field imidazole ligands ($\tau = 6-50$ ps). The absence of a $(P^{\bullet+})Zn^{II}$ signal that would complement photoinduced PCET at the $PFe^{III}-OH$ subunit (i.e., $PFe^{III}-OH \rightarrow PFe^{II}-OH_2$) shows that excitation energy transfer and intersystem crossing channels dominate the quenching, regardless of whether proximal strong field ligands are present. Moreover, this photophysical assignment is independent of the solvent dielectric constant and whether a phenylene or biphenylene spacer is used to span the two porphyrin subunits. Electronic structure calculations suggest that the structural reorganization attendant to reductive PCET at the high-spin $Fe^{III}-OH$ center imposes a severe kinetic cost that can only be alleviated by inducing a low-spin electronic configuration with two strong-field axial ligands.

Introduction

Zinc(II) porphyrins (PZn^{II}) and iron(III) porphyrins (PFe^{III}) are complementary chromophores for investigations of electron transfer (ET) in biological and chemical charge transport networks. The incorporation of the d^{10} Zn(II) ion into a porphyrin engenders a singlet excited state from which an electron is dispatched to PFe^{III}.[1] In protein−protein complexes, in which one of the proteins is a heme, ET may thus be phototriggered by replacement of the heme iron with zinc.[2−7] The distance and orientation of the porphyrin chromophores are fixed by the secondary and tertiary environment of the protein scaffolds.

Outside of the protein environment, the PZn^{II} and PFe^{III} chromophores may be positioned by appending them to the rigid spacers.[8−17] In many of these dyads, the PFe^{III} acceptor center is coordinated by a weak field (WF) ligand, such as Cl^-, to yield a five-coordinate $PFe^{III}Cl$ center. Electron transfer has been inferred in such dyads by the efficient quenching of the PZn^{II} singlet excited state.[8−10] Transient absorption (TA) features may also be used to measure ET in $PZn^{II}-PFe^{III}Cl$ dyads. Because TA spectral signatures arising from the PFe^{II} versus that of the PFe^{III} center in which the axial halide has dissociated are similar, the establishment of ET in $PZn^{II}-PFe^{III}$ dyads has focused primarily on observing the TA features of the electron-transfer product of the donor, $(P^{\bullet+})Zn^{II}$. This species has been observed, but only when the iron center is six-coordinate and axially ligated by strong field (SF) ligands, such as imidazole (Im).[13−16] Compelling evidence for this contention has been provided by comparative TA spectra of five-coordinate $PFe^{III}Cl$ and six-coordinate $PFe^{III}(Im)_2$ in the wavelength region of $(P^{\bullet+})Zn^{II}$.[16] The five-coordinate $PZn^{II}-PFe^{III}Cl$ dyads show no absorption in the $(P^{\bullet+})Zn^{II}$ region, excluding the assignment of ET. The S_1 quenching of PZn^{II} in the dyad is assigned to electronic energy transfer (EET) and accelerated intersystem crossing (ISC),[16,17] which had been postulated to increase on account of the proximity of the paramagnetic Fe center.[11,18,19] When Im is added to five-coordinate $PZn^{II}-PFe^{III}Cl$ dyads to generate $PZn^{II}-(Im)_2-PFe^{III}(Im)$, the TA signal for $(P^{\bullet+})Zn^{II}$ is observed, thus providing direct evidence for the charge-separated state. The conclusion of these studies is that ET predominates when the Fe center adopts the low-spin configuration by binding two SF ligands, such as Im. For the high-spin iron of five-coordinate $PFe^{III}Cl$ centers, ET cannot compete with EET and ISC.

The linchpin between the five-coordinate $PFe^{III}(WF)$ and six-coordinate $PFe^{III}(SF)_2$ endpoints is the mixed ligand, six-coordinate $PFe^{III}(WF)(SF)$ complex. Is the addition of a sixth strong field ligand sufficient to switch the excited-state reactivity of $PZn^{II}-PFe^{III}$ dyads from EET to ET? The answer to this question is essential to charge transport in biology, especially when that transport involves an electron and proton to activate oxygenated substrate at a heme cofactor. The heme centers of mono-oxygenases typically are axially coordinated by the weak field ligand of oxygen and a strong field ligand, such as histidine. The active oxidation catalysts, Compound I ($(P^{\bullet+})Fe^{IV}=O$) and Compound II ($PFe^{IV}=O$), respectively, of heme enzymes such as cytochrome P450[20−24] and cytochrome *c* peroxidase,[25−29] can be generated upon oxidation of ferric hydroxy species ($PFe^{III}-OH$) coupled to deprotonation,[30,31] or by protonation of a ferric peroxy species followed by loss of water.[32,33] Interconversion between O_2 and H_2O in cytochrome *c* oxidase cycles through metal aquo ↔ hydroxo ↔ oxo species, in which the redox changes at the metal are managed along ET pathways that are distinct from that for management of the proton.[34,35] Electrons transfer into and out of active sites over long distances in concert with protons that hop to or from the active site along amino acid side chains or along structured water channels. The case

10.1021/jp070447v CCC: $37.00
Published on Web 06/23/2007

CHART 1

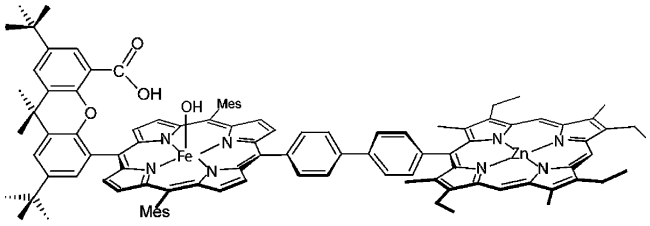

1

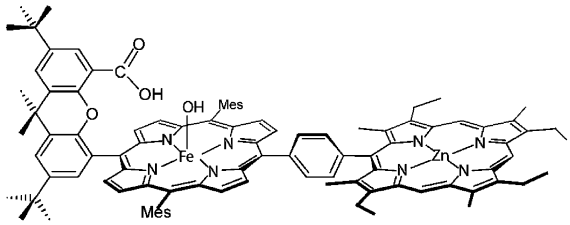

2

of bidirectional PCET is more frequent than might be expected because the evolution of this pathway permits enzymes to manage the disparate length scales for ET and PT to be satisfied so that the electron and proton can couple for the catalytic activation of substrate and radical transport.[36,37]

The construction of $PFe^{III}(WF)(SF)$ species is required of models of such orthogonal charge transport in biology. Generating a mixed-ligand $PFe^{III}(WF)(SF)$ species requires a specifically engineered distal coordination site to avert formation of the thermodynamically favored $PFe^{III}(SF)_2$ species.[38−40] The aforementioned redox active heme enzymes such as peroxidases have evolved tertiary structures that place strong-field, nitrogen-donor ligands such as histidine in the proximal position, leaving the distal coordination site available for substrate activation via redox reactions.[41−44] We have captured this biological design principle with Hangman porphyrins, in which an acid−base group is positioned over a PFe^{III}−OH platform via a xanthene or dibenzofuran spacer.[45−48] The hydroxide ligand is stabilized by its incorporation into a hydrogen bond network connected to the hanging group,[47] and it is sterically protected by the acid−base functionality hanging over the face of the porphyrin. In this way, the fifth coordination site of a PFe^{III} platform can be fixed with a WF PCET-active ligand. A $PFe^{III}(WF)(SF)$ species can be obtained by the addition of a SF ligand, and a dyad may be established by installing a PZn^{II} photoreductant at a fixed distance via a spacer, as shown by the Hangman porphyrin dyads in Chart 1. The systems consist of a Fe^{III}−OH Hangman porphyrin attached via a variable spacer to a Zn(II) etio-I porphyrin photoreductant ($(E\text{-}P)Zn^{II}$) via a biphenylene (dyad **1**) or phenylene spacer (dyad **2**). In both cases, a carboxylic acid group is suspended over the hydroxide ligand via a xanthene pillar. The $PFe^{III}(WF)(SF)$ adducts are readily formed in solution in the presence of strong-field Im ligands. We now report the first transient kinetics studies of Hangman porphyrin dyads in both $PFe^{III}(WF)$ and $PFe^{III}(WF)(SF)$ coordination states.

Experimental Section

Materials. Silica gel 60 (70−230 and 230−400 mesh, Merck) and aluminum oxide 60 (EM Science) were used for column chromatography. Solvents for synthesis were reagent grade or better and were dried according to standard methods.[49] Spectroscopic experiments employed distilled THF or toluene. All other reagents were used as received. Porphyrins were synthesized by standard methods. 4,5-Dibromo-2,7-di-*tert*-butyl-9,9-dimethylxanthene was obtained from Sigma-Aldrich. Previously published procedures were employed for the preparation of 4-methoxycarbonyl-5-bromo-2,7-di-*tert*-butyl-9,9-dimethylxanthene (**3**),[45] zinc(II) 5,15-dimesityl-10-(4′,4′,5′,5′-tetramethyl-[1′,3′,2′](dioxaborolan-2′-yl)porphyrin (**4**),[50] and Hangman monomers $(HPX)Fe^{III}$−OH (HPX = Hangman porphyrin xanthene),[45] $(TMP)Fe^{III}$−OH (TMP = tetramesityl porphyrin),[45] and $(E\text{-}P)Zn^{II}$.[51]

5-[4-(5-Methoxycarbonyl-2,7-di-*tert*-butyl-9,9-dimethylxanthenyl)]-10,20-dimesityl Porphyrin (5). Zinc(II) 5,15-dimesityl-10-(4′,4′,5′,5′-tetramethyl[1′,3′,2′] dioxaborolan-2′-yl)-porphyrin (**4**) (328 mg, 0.446 mmol), 4-methoxycarbonyl-5-bromo-2,7-di-*tert*-butyl-9,9-dimethylxanthene (**3**) (213 mg, 0.446 mmol), $Pd(PPh_3)_4$ (100 mg, 0.086 mmol), and Na_2CO_2 (150 mg) were mixed in a Schlenk flask and purged with N_2.[45−47,52] DMF (60 mL) and water (6 mL) were added under N_2, and the reaction was heated for 18 h at 90 °C. Water (50 mL) was added to the reaction mixture, and the product was extracted with dichloromethane (3 × 50 mL). The combined dichloromethane extracts were washed with water to remove residual DMF. The dichloromethane solution was treated with HCl (25 mL, 6 M, aq) to remove zinc. After 10 min, the HCl phase was removed, and the dichloromethane phase was washed with water (3 × 25 mL). The organic phase was dried over $MgSO_4$ and purified by chromatography (SiO_2, dichloromethane/hexane 1:2) to furnish the title compound (175 mg, 0.19 mmol, 42%). ^{1}H NMR (500 MHz, CDCl3, 25 °C), δ/ppm: −2.0 (2H, s, NH), −0.49 (3H, s, COOMe), 1.27 (9H, s, *t*-Bu), 1.54 (9H, s, *t*-Bu), 1.88 (6H, s, 2 × CH_3), 1.96 (12H, s, 4 × CH_3), 2.67 (6H, s, 2 × CH_3), 7.31 (1H, d, J = 4.5 Hz, ArH), 7.32 (2H, s, ArH), 7.35 (2H, s, ArH), 7.66 (1H, d, J = 4.5 Hz, ArH), 7.90 (1H, d, J = 4.5 Hz, ArH), 8.03 (1H, d, J = 4.5 Hz, ArH), 8.75 (2H, d, J = 4.5 Hz, β-H), 8.85 (2H, d, J = 4.5 Hz, β-H), 8.88 (2H, d, J = 4.5 Hz, β-H), 9.32 (2H, d, J = 4.5 Hz, β-H), 10.17 (1H, s, *meso*-H).

5-[4-(5-Methoxycarbonyl-2,7-di-*tert*-butyl-9,9-dimethylxanthenyl)]-10,20-dimesityl-15-bromoporphyrin (6). *N*-Bromosuccinimide (30 mg, 0.168 mmol) was added to a solution of porphyrin (**5**) (127 mg 0.137 mmol) in $CHCl_3$ (50 mL),[50] and the reaction was stirred at RT for 2 h 45 min. The solvent was evaporated, and the product purified by chromatography (SiO_2, dichloromethane) to furnish **6** (135 mg, 0.134 mmol, 98%). ^{1}H NMR (400 MHz, $CDCl_3$, 25 °C), δ/ppm: −2.46 (2H, s, NH), −0.40 (3H, s, COOMe), 1.24 (9H, s, *t*-Bu), 1.50 (9H, s, *t*-Bu), 1.84 (6H, s, 2 × CH_3), 1.90 (6H, s, 2 × CH_3), 1.91 (6H, s, 2 × CH_3), 2.64 (6H, s, 2 × CH_3), 7.28 (1H, d, J = 2.4 Hz, ArH), 7.283 (2H, s, ArH), 7.30 (2H, s, ArH), 7.62 (1H, d, J = 2.4 Hz, ArH), 7.85 (1H, d, J = 2.4 Hz, ArH), 7.96 (1H, d, J = 2.4 Hz, ArH), 8.62 (2H, d, J = 4.8 Hz, β-H), 8.73 (2H, d, J = 4.8 Hz, β-H), 8.76 (2H, d, J = 4.8 Hz, β-H), 9.62 (2H, d, J = 4.8 Hz, β-H).

5-[4-(5-Hydroxycarbonyl-2,7-di-*tert*-butyl-9,9-dimethylxanthenyl)]-10,20-dimesityl-15-bromoporphyrin (7). Compound **6** (55 mg, 55 μmol) was dissolved in THF, and NaOH (aq, 20%, 10 mL) was added. N_2 was bubbled through the reaction mixture for 10 min before the reaction was heated to reflux under N_2 for 3 days. The organic phase was separated and washed with water. The solvent was evaporated and the product purified by chromatography (SiO_2, ethyl acetate/hexane 3:7) to furnish **7** (37 mg, 37 μmol, 67%). ^{1}H NMR (400 MHz, CD_2Cl_2, 25 °C), δ/ppm: −2.54 (2H, s, NH), 0.88 (1H, s, br, COOH), 1.25 (9H, s, *t*-Bu), 1.53 (9H, s, *t*-Bu), 1.83 (6H, s, 2 × CH_3), 1.87 (6H, s, 2 × CH_3), 1.93 (6H, s, 2 × CH_3), 2.62 (6H, s, 2 × CH_3), 7.30 (2H, s, ArH), 7.31 (2H, s, ArH), 7.60 (1H, d,

J = 2.4 Hz, ArH), 7.75 (1H, d, J = 2.4 Hz, ArH), 7.96 (1H, d, J = 2.4 Hz, ArH), 8.11 (1H, d, J = 2.4 Hz, ArH), 8.62 (2H, d, J = 4.8 Hz, β-H), 8.73 (2H, d, J = 4.8 Hz, β-H), 8.75 (2H, d, J = 4.8 Hz, β-H), 9.65 (2H, d, J = 4.8 Hz, β-H). ES MS m/z [M^+]: calcd 988.39; found 990.23.

5-(4-[4′,4′,5′,5′-Tetramethyl[1′,3′,2′]dioxaborolan-2′-]phenyl)-2,8,13,17-tetraethyl-3, 7,12,18-tetramethylporphyrin (8). Zn(II) 5-(4-bromophenyl)-etio-porphyrin[53,54] (386 mg, 0.55 mmol), bis(pinacolato)diboron (154 mg, 0.605 mmol), $PdCl_2$(dppf) (15 mg, 0.02 mmol), and CH_3COOK (196 mg, 2 mmol)[55,56] were mixed in a Schlenk flask and purged with N_2. DMSO (4 mL) was added under N_2, and the reaction mixture was freeze/pump/thawed twice under N_2 before being heated for 16 h at 100 °C. Water (20 mL) was added, and the product was extracted with dichloromethane (3 × 25 mL). The combined dichloromethane extracts were evaporated, and the crude product was purified by chromatography (SiO_2, dichloromethane/hexane 3:1) to furnish **8** (275 mg, 0.37 mmol, 67%). ^{1}H NMR (400 MHz, CD_2Cl_2, 25 °C), δ/ppm: 1.52 (12H, s, 4 × CH_3), 1.76 (6H, t, J = 7.6 Hz, 2 × CH_3), 1.86 (6H, t, J = 7.6 Hz, 2 × CH_3), 2.45 (6H, s, 2 × CH_3), 3.60 (6H, s, 2 × CH_3), 3.98−4.07 (8H, m, 4 × CH_2), 8.12 (4H, dd, J = 7.6, 26.4 Hz, PhH), 9.94 (1H, s, *meso*), 10.11 (2H, s, *meso*-H).

Zn(II) *p*-Chlorobiphenyl-etio-porphyrin (9). DMF (1 mL) was added to K_2CO_3 (27 mg, 200 μmol), and water was added until the solid dissolved. Porphyrin **8** (50 mg, 67 μmol), *p*-iodochlorobenzene (16 mg, 67 μmol), $Pd(PPh_3)_4$ (7.7 mg, 6.7 μmol), and finally toluene (1 mL) were added. The reaction mixture was freeze/pump/thawed twice under N_2 before being heated for 23 h at 90 °C. DMF was removed by extraction with water, the toluene phase was evaporated, and the crude product was purified by chromatography (SiO_2, dichloromethane) to furnish **9** (43 mg, 59 μmol, 88%). ^{1}H NMR (400 MHz, $CDCl_3$, 25 °C), δ/ppm: 1.78 (6H, t, J = 7.6 Hz, 2 × CH_3), 1.91 (6H, t, J = 7.6 Hz, 2 × CH_3), 2.54 (6H, s, 2 × CH_3), 3.66 (6H, s, 2 × CH_3), 4.04 (4H, q, J = 7.6 Hz, 2 × CH_2), 4.10 (4H, q, J = 7.6 Hz, 2 × CH_2), 7.60 (2H, d, J = 8.4 Hz, PhH), 7.92 (2H, d, J = 8.4 Hz, PhH), 7.98 (2H, d, J = 8.0 Hz, PhH), 8.16 (2H, d, J = 8.0 Hz, PhH), 10.05 (1H, s, *meso*-H), 10.17 (2H, s, *meso*-H). ES MS m/z [M^+]: calcd 726.25; found 726.3.

Zn(II) *p*-[4′,4′,5′,5′-Tetramethyl[1′,3′,2′]dioxaborolan-biphenyl-etio-porphyrin (10). Compound **9** (30 mg, 41 μmol), pinacoldiboron (12 mg, 45 μmol), $Pd(PCy_3)_2$ (5 mg, 7.5 μmol), and CH_3COOK (6 mg, 61.5 μmol) were mixed in a Schlenk flask and purged with N_2. Dioxane (dry, 0.5 mL) was added, and the reaction mixture was freeze/pump/thawed twice under N_2 before being heated for 5 days at 80 °C. Dioxane was evaporated, and the crude product was purified by chromatography (SiO_2, dichloromethane/hexane 1:3) to furnish **10** (9 mg, 11 μmol, 27%). ^{1}H NMR (400 MHz, CD_2Cl_2, 25 °C), δ/ppm: 1.52 (12H, s, 4 × CH_3), 1.78 (6H, t, J = 7.6 Hz, 2 × CH_3), 1.91 (6H, t, J = 7.6 Hz, 2 × CH_3), 2.55 (6H, s, 2 × CH_3), 3.66 (6H, s, 2 × CH_3), 4.05 (4H, q, J = 7.6 Hz, 2 × CH_2), 4.13 (4H, q, J = 7.6 Hz, 2 × CH_2), 7.60 (2H, d, J = 8.4 Hz, PhH), 7.95 (2H, d, J = 8.4 Hz, PhH), 8.01 (2H, d, J = 8.4 Hz, PhH), 8.15 (2H, d, J = 8.4 Hz, PhH), 10.11 (1H, s, *meso*-H), 10.21 (2H, s, *meso*-H). ES MS m/z [M^+]: calcd 818.37; found 817.29

Porphyrin Dyad (11). Compound **10** (18 mg, 22 μmol), **7** (18 mg, 18 μmol), $PdCl_2$(dppf), and K_2CO_3 (34 mg, 246 μmol) were mixed in a Schlenk flask and purged with N_2. DMF (0.5 mL), toluene (1 mL), and water (0.1 mL) were added, and the reaction mixture was freeze/pump/thawed twice under N_2 before being heated for 19 h at 90 °C. DMF was removed by extraction with water, the toluene phase was evaporated, and the crude product was purified by chromatography (SiO_2, dichloromethane gradient dichloromethane/diethyl ether 1:1) to furnish **11** (17 mg, 11 μmol, 58%). ^{1}H NMR (400 MHz, CD_2Cl_2, 25 °C), δ/ppm: −2.44 (2H, s, NH), 1.30 (9H, s, *t*-Bu), 1.62 (9H, s, *t*-Bu), 1.88 (6H, t, J = 7.6 Hz, 2 × CH_3), 1.93 (12H, t, J = 7.6 Hz, 4 × CH_3), 1.97 (6H, s, 2 × CH_3), 1.99 (6H, s, 2 × CH_3), 2.68 (6H, s, 2 × CH_3), 2.73 (6H, s, 2 × CH_3), 3.70 (6H, s, 2 × CH_3), 4.12 (4H, q, J = 7.6 Hz, 2 × CH_2), 4.14 (4H, q, J = 7.6 Hz, 2 × CH_2), 7.37 (4H, s, ArH), 7.65 (1H, d, J = 2.4 Hz, ArH), 7.80 (1H, d, J = 2.4 Hz, ArH), 8.02 (1H, d, J = 2.4 Hz, ArH), 8.28 (1H, d, J = 2.4 Hz, ArH), 8.3 − 8.50 (8H, m, PhH), 8.75 (2H, d, J = 4.8 Hz, β-H), 8.85 (4H, m, β-H), 9.11 (2H, d, J = 4.8 Hz, β-H), 10.06 (1H, s, *meso*-H), 10.24 (1H, s, *meso*-H). ES MS m/z [M^+]: calcd 1600.75; found 1600.86.

Zn−Fe Porphyrin Dyad (1). $FeBr_2$ (40 mg, 185 μmol), and porphyrin dyad **11** (8 mg, 6 μmol) were mixed in a Schlenk flask and purged with N_2. THF (1 mL) and collidine (0.1 mL) were added to the flask, and the reaction was heated to 40 °C overnight under N_2. The reaction mixture was then shaken with NaOH (2 mL, 10% aq) for 10 min. The product was extracted with dichloromethane (3 × 15 mL). The combined organic extracts were evaporated, and the crude product was purified by chromatography (SiO_2, dichloromethane gradient dichloromethane/diethyl ether 1:1). Final treatment with $Zn(COOCH_3)_2$ (carried out in order to replenish any Zn lost during workup and purification) furnished dyad **1** (3.5 mg, 2.1 μmol, 35%). ES MS m/z: [M − OH] and [M^+]: calcd 1654.67 and 1671.67; found 1653.37 and 1668.38, respectively.

Porphyrin Dyad (12). DMF (1 mL) was added to K_2CO_3 (39 mg, 280 μmol), and water was added dropwise until the solid dissolved. After the K_2CO_3 was dissolved, Hangman porphyrin carboxylate (**7**) (20.5 mg, 20.7 μmol), Zn(II) 4-pinacolatophenyl-etio-porphyrin (**8**) (19.5 mg, 26.2 μmol), and $PdCl_2$(dppf) (5 mg, 6.8 μmol) were added; and, finally, toluene (2 mL) was added, and the reaction was freeze/pump/thawed twice under N_2 before being heated for 22 h at 90 °C. DMF was removed by extraction with water. The toluene phase was evaporated, and the crude product was purified by chromatography (SiO_2, dichloromethane/hexane 2:1 gradient to dichloromethane with 3% diethyl ether) to furnish dyad **12** (27 mg, 18 μmol, 85%). ^{1}H NMR (400 MHz, CD_2Cl_2, 25 °C), δ/ppm: −2.34 (2H, s, NH), 0.88 (1H, s, br, COOH), 1.30 (9H, s, *t*-Bu), 1.63 (9H, s, *t*-Bu), 1.86 (6H, t, J = 7.6 Hz, 2 × CH_3), 1.91 (6H, t, J = 7.6 Hz, 2 × CH_3), 1.98 (6H, s, 2 × CH_3), 2.0 (6H, s, 2 × CH_3), 2.02 (6H, s, 2 × CH_3), 2.70 (6H, s, 2 × CH_3), 3.09 (6H, s, 2 × CH_3), 3.60 (6H, s, 2 × CH_3), 3.97 (4H, q, J = 7.6 Hz, 2 × CH_2), 4.14 (4H, q, J = 7.6 Hz, 2 × CH_2), 7.40 (4H, s, ArH), 7.66 (1H, d, J = 2.4 Hz, ArH), 7.80 (1H, d, J = 2.4 Hz, ArH), 8.03 (1H, d, J = 2.4 Hz, ArH), 8.30 (1H, d, J = 2.4 Hz, ArH), 8.48 − 8.46 (2H, m, PhH), 8.76−8.66 (2H, m, PhH), 8.80 (2H, d, J = 4.8 Hz, β-H), 8.88 (2H, d, J = 4.4 Hz, β-H), 8.99 (2H, d, J = 4.4 Hz, β-H), 9.41 (2H, d, J = 4.8 Hz, β-H), 9.76 (1H, s, *meso*-H), 10.11 (2H, s, *meso*-H). ES MS m/z [M + Zn + CH_3] and [M^+]: calcd 1600.65 and 1524.72, respectively; found 1603.62 and 1528, respectively.

Zn−Fe Porphyrin Dyad (2). $FeBr_2$ (25 mg, 116 μmol) was added to a degassed solution of porphyrin dyad **12** (9.2 mg, 6 μmol) in THF (1 mL) and collidine (0.1 mL) and the mixture was refluxed under N_2 for 3 h. The reaction mixture was then shaken with NaOH (2 mL, 10% aq) for 10 min. The product was extracted with dichloromethane (3 × 15 mL), the combined organic extracts were evaporated, and the crude product was purified by chromatography (SiO_2, dichloromethane gradient dichloromethane/diethyl ether 1:1). Final treatment with Zn-

$(COOCH_3)_2$ (vide supra) furnished dyad **2** (3.5 mg, 2.1 μmol, 35%). ES MS *m*/*z* [M − OH] and [M^+]: calcd 1578.64 and 1595.64, respectively; found 1577.70 and 1595, respectively.

Physical Methods. NMR spectra were recorded at the MIT Department of Chemistry Instrumentation Facility (DCIF) on a Varian Mercury 300 Varian Inova 500 spectrometer and a Bruker Avance-400 NMR spectrometer. All chemical shifts are reported using the standard δ notation in parts-per-million; positive chemical shifts are to higher frequency from the given reference. Mass spectral analyses were performed at the MIT DCIF on a Bruker Omniflex MALDI-TOF and a Bruker Daltonics APEXIV 4.7 T Fourier transform ion cyclotron resonance mass spectrometer (FT-ICR-MS).

Spectroscopy. All optical spectroscopy was performed at room temperature. Absorption spectra were obtained using a Spectral Instruments 440 Series spectrophotometer. Samples for transient absorption experiments were contained within a 2-mm path length, clear, fused-quartz cell at concentrations of $\sim 1.5 \times 10^{-5}$ M to give an optical density of $\sim$1.2 at 405 nm. Picosecond TA measurements were performed on a chirped-pulse amplified Ti:sapphire laser system as we have previously described.[57,58] Briefly, the 810-nm output beam was split, with the majority component frequency-upconverted to produce 100-fs excitation pulses of the desired wavelength in an optical parametric amplifier (or simply frequency-doubled to produce 405-nm excitation in some cases). A minor component of the 810-nm beam was focused on a sapphire substrate to generate a visible continuum probe pulse. The excitation power was attenuated to $\sim$3−6 μJ/pulse and focused in the sample to overlap collinearly with the probe beam, which was polarized at the magic angle ($\theta_m = 54.7°$) relative to the excitation beam. Time resolution was achieved by propagating the excitation beam along a computer-controlled, optical delay line. For single-wavelength kinetic measurements, the optical delay line repeatedly sampled a series of delay times, and the pump beam was mechanically chopped at $\omega = 500$ Hz. The probe beam was spectrally resolved in the spectrometer, a single wavelength was selected, and the signal was measured on a photodiode and amplified with a lock-in amplifier at the 500-Hz excitation frequency. TA spectra were recorded at discrete times by coupling the probe beam exiting the sample into a liquid light guide to homogenize the beam spatially. The spectrum was then resolved in the monochromator (ISA Instruments, TRIAX 320) and recorded on a CCD camera (Andor Technology). The reference spectrum was taken at negative time. For the transient emission experiments, we used a Hamamatsu Streak-scope (C4334) that has been described elsewhere.[59] Steady-state fluorescence spectra were recorded on an automated Photon Technology International QM 2001-4 fluorometer that is equipped with a 150-W Xe arc lamp and a Hamamatsu R928 photomultiplier tube.

Computational Methods. DFT calculations were performed using the Amsterdam Density Functional (ADF2002.02) program[60,61] on a home-built Linux cluster comprising 60 Intel processors organized in groups of 12 running in parallel. The generalized gradient approximation was used as implemented in ADF by the Becke-88 functional for exchange,[62] and the Perdew−Wang-91 functional for correlation.[63] A basis set of triple-ζ with polarization was used for Fe, O, and N atoms, and double-ζ with polarization was used for other atoms with the frozen core approximation. The input coordinates for the PFe^{III}−OH geometry optimization were obtained from the X-ray crystal structure of $(HPX)Fe^{III}$−OH with all meso substituents replaced with hydrogen atoms for computational expediency. Geometry optimization was carried out with S = 5/2 with spin restriction lifted. The output coordinates of the above calculation were adapted as input for the $PFe^{II}-OH_2$ geometry optimization. Geometry optimization was carried out with S = 2 with spin restriction lifted.

Results

The designs of dyads **1** and **2** were based on reports of photoinduced ET from PZn^{II} donors to PFe^{III} acceptors in fixed-distance ET studies of analogous model systems that lack the Hangman functionality.[8−17] PZn^{II} photoreductants present well-defined spectroscopic signatures that can be used to kinetically resolve ET and PCET reactions.[14,16,58,64−69] The Hangman constituents, namely, the carboxylic acid appended to a xanthene pillar, were selected on the basis of the favorable geometry they impart for PCET at the hydroxide ligand, as revealed in the X-ray structure[47] and proven in PCET reactivity studies with Hangman metalloporphyrin monomers.[45,46,48]

The Hangman porphyrin dyads **1** and **2** are synthesized by a series of palladium-catalyzed Suzuki couplings, as outlined in Scheme 1. The porphyrin subunits and the Hangman functionality are synthesized separately, metalated (if required), and coupled under standard Suzuki conditions. We note that in the construction of the Hangman dyads, hydrolysis of the ester (**6**) is carried out prior to coupling with the $(E\text{-}P)Zn^{II}$ subunit because Zn(II) is easily lost under hydrolysis conditions. The asymmetry of the porphyrin dyads requires that the E-P subunits (**8** and **10**) contain Zn(II) prior to palladium-catalyzed Suzuki coupling[70] with the free-base Hangman porphyrin **7**, since selective metalation of a free-base dyad is not possible. The resulting dyad can be characterized by NMR spectroscopy prior to metalation with iron(II) bromide. An alternative strategy is to first metalate Hangman porphyrin **7** with iron(II) bromide and then undertake a Suzuki coupling between the metalated Hangman porphyrin and etio porphyrin **8** or **10**. This method has the advantage that the tightly bound iron atom would not be removed under the reaction conditions or workup. However, on the other hand, iron porphyrins are more difficult to purify and characterize by NMR, and the Suzuki coupling leads to several compounds. Hence, we followed the modular approach developed in Scheme 1, which permits the ET and PT distances to be readily adjusted through variation of the spacer and the Hangman pillar, respectively. Additionally, the nature of the hanging acid group and the central metal can be easily varied.

The photophysical properties of dyads **1** and **2** were first characterized in the absence of SF ligands. Figure 1 reproduces the electronic absorption spectra of **1**, $(HPX)Fe^{III}$−OH and $(E\text{-}P)Zn^{II}$. The absorption spectrum of **1** is well approximated by the sum of the spectra of the constituent monomers. The absorption profile is dominated by sharp Soret ($\lambda_{abs,max}$ = 409 nm) and Q bands ($\lambda_{abs,max}$ = 535 and 571 nm), all originating from the $\pi-\pi^*$ transitions of the $(E\text{-}P)Zn^{II}$ component. The $(HPX)Fe^{III}$−OH component contributes broader and weaker features across the spectrum due to the lower symmetry and mixing of charge transfer (CT) transitions involving the half-filled d-orbital manifold.[1,71] The most notable disparity between the spectrum of **1** and that obtained from the sum of the constituent monomers is that the Soret band of **1** is red-shifted by $\sim$4 nm. This is most likely due to the biphenylene bridge of **1**, which is expected to electronically perturb the $(E\text{-}P)Zn^{II}$ chromophore, weak excitonic interaction between the two adjacent porphyrin chromophores,[72] or both.

The spectra in Figure 1 reveal λ = 405 nm as a suitable excitation wavelength for the selective excitation of the

SCHEME 1

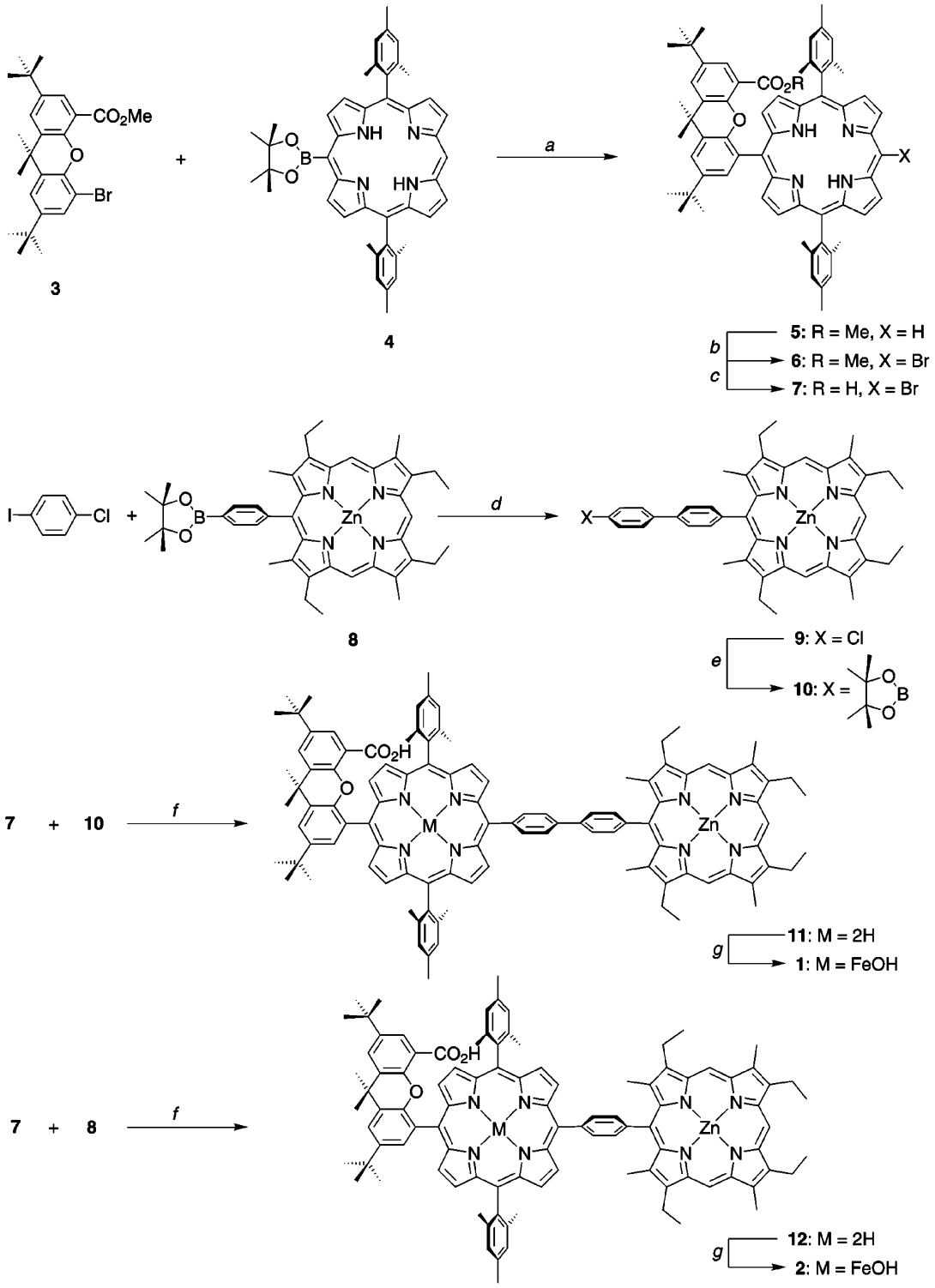

(*a*) $Pd(Ph_3P)_4$, Na_2CO_3, DMF/H_2O; (*b*) NBS, $CHCl_3$; (*c*) NaOH (aq), THF (*d*) $Pd(Ph_3P)_4$, K_2CO_3, DMF/H_2O/tolune; (*e*) $Pd(PCy_3)_2$, CH_3COOK, Dioxane; (*f*) $PdCl_2$(dppf), K_2CO_3, DMF/H2O/toluene; (*g*) 1) $FeBr_2$/THF/Collidine 2)NaOH (aq).

(E-P)Zn^{II} donor in transient laser studies. The (E-P)Zn^{II} subunit contributes >85% to the optical density of the dyad at this wavelength. Rapid internal conversion in PZn^{II} species is expected to deliver the S_1 excited state within ~1 ps.[73,74] Alternatively, the S_1 excited state can be furnished directly by excitation into the $Q_{0,0}$ absorption band at $\lambda = 570$ nm, where the (E-P)Zn^{II} contributes >90% to the total optical density of the dyad. Direct excitation of the (HPX)Fe^{III}−OH, owing to its residual absorbance at $\lambda = 405$ and 570 nm, offers little interference to the dynamics of the dyad system, since PFe^{III}-(X) photophysics establishes that heme iron excited states decay by nonradiative relaxation on picosecond timescales.[1,75−78]

Given that (E-P)Zn^{II} can be selectively excited, the S_1 excited-state lifetime of (E-P)Zn^{II} in the dyad is a critical determinant for the time evolution of subsequently generated intermediates. Initial experiments sought to measure the excited-state lifetime of (E-P)Zn^{II} within the dyad using transient emission (TE) spectroscopy. As a benchmark, visible excitation of monomeric

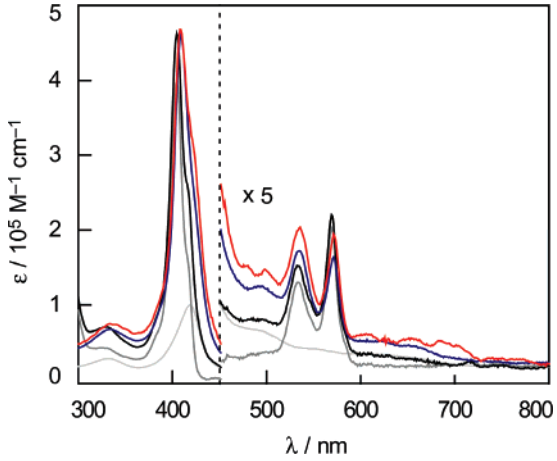

Figure 1. Electronic absorption spectra of dyad **1** (blue), dyad **2** (red), the (HPX)Fe^{III}−OH monomer (light gray), the (E-P)Zn^{II} (dark gray) monomer, and the sum of constituent monomers (black). All spectra were recorded in toluene.

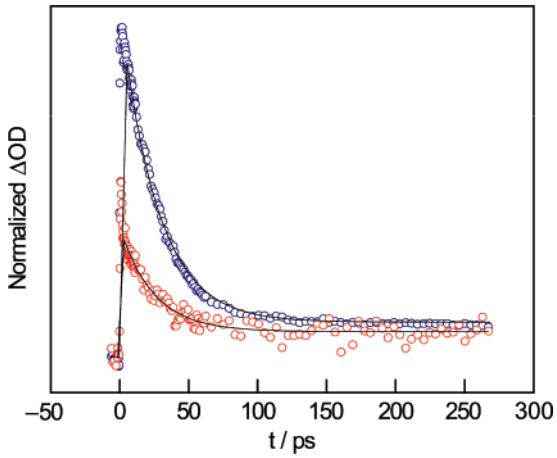

Figure 2. TA kinetics for dyad **1** in toluene with $\lambda_{exc} = 405$ nm and $\lambda_{probe} = 460$ nm (blue circles) and 660 nm (red circles). Monoexponential fits are also shown.

(E-P)Zn^{II} results in fluorescence from the S_1 state ($\lambda_{em,max} =$ 572 and 627 nm) with a lifetime of $\tau = 1.8$ ns and a quantum yield of $\Phi \sim 0.045$ (estimated as being equal to the fluorescence quantum yield of the electronically and structurally similar (OEP)Zn^{II}).[79] In the absence of a reaction pathway, the predominant fate of S_1 is ISC to a long-lived and nonemissive triplet state (T_1), which is ~0.4 V less reducing than S_1.[80] However, the (E-P)Zn^{II} moiety of **1** exhibited no detectable fluorescence, even with excitation powers approaching 5 μJ/pulse (either $\lambda_{exc} = 405$ or 570 nm). This result suggests that quenching of S_1 is particularly rapid.

In the absence of an observable fluorescence signal, TA spectroscopy was required to measure the S_1 lifetime and to monitor the signatures of transient intermediates directly. The S_1 excited state of PZn^{II} exhibits a strong characteristic TA feature at $\lambda = 430-500$ nm, making this a suitable region to probe the S_1 lifetime. Figure 2 shows the TA kinetics obtained for **1** with $\lambda_{exc} = 405$ nm and $\lambda_{probe} = 460$ nm (blue circles). The data is fit well by a monoexponential decay function with a time constant of $\tau = 25(3)$ ps. The rapidity of the decay is consistent with the lack of emission for the complex. Using the natural S_1 lifetime of (E-P)Zn^{II}, the fluorescence quantum yield is determined to be $\Phi \sim 7 \times 10^{-4}$. The same result is obtained when $\lambda_{exc} = 570$ nm, providing further support for the participation of the S_1 (rather than the S_2) excited state of the (E-P)Zn^{II}.

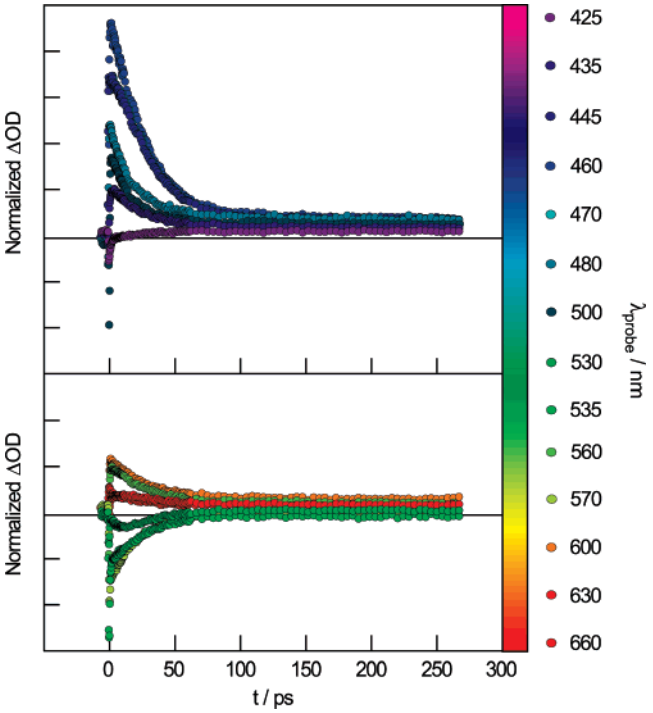

Figure 3. TA kinetics for dyad **1** in toluene with $\lambda_{exc} = 405$ nm and visible probes indicated.

TA experiments were subsequently performed with probe wavelengths targeting potential PCET intermediates. Red probe wavelengths were employed because (E-$P^{\bullet+}$)Zn^{II}, which is the expected photo-oxidation product, has a distinctive absorption feature in the $\lambda = 630-700$ nm region, an otherwise clear spectral window in $PZn^{II}-PFe^{III}$ dyads.[14,16,58,64−69] Figure 2 shows the TA kinetics obtained for **1** with $\lambda_{probe} = 660$ nm (red circles) and $\lambda_{exc} = 405$ nm. An initial rapid decay component of $\tau \sim 2$ ps is followed by a monoexponential decay of $\tau =$ 25(5) ps. This observation is consistent with the observed 25-ps quenching lifetime of the S_1 excited state. However, the absence of a rising TA signal at this wavelength on the time scale of S_1 depletion implies that PCET is not the dominant quenching mechanism of the S_1 excited state.

The reduction of (HPX)Fe^{III}−OH is less easily observed because anticipated spectral shifts for this chromophore occur in regions where the S_1, T_1 and radical cation states of PZn^{II} absorb strongly. The difference absorption spectra of various Fe(II) porphyrins, including (HPX)Fe^{II}, exhibit a shoulder on the red edge of the Soret band ($\lambda_{abs,max} = 442$ nm) and bleaching of the broad absorbance associated with the corresponding Fe(III) porphyrin in the $\lambda = 450-500$-nm region.[81,82] The TA kinetics collected in this wavelength range (Figures 2 and 3) show no evidence of a bleach attributable to PFe^{II} generation. On the other hand, the strong positive signals that are observed are associated with the PZn^{II} component and decay at the S_1 lifetime ($\tau = 25(5)$ ps), suggesting that PZn^{II} signatures would obscure those of PFe^{II} generation whether or not PCET was operative.

Kinetic profiles were obtained with probe wavelengths extending across the visible spectrum, as shown in Figure 3. Positive signals that decay monoexponentially ($\tau = 25(5)$ ps), when considered beyond the first few picoseconds of vibrational cooling) were observed at most wavelengths ($\lambda_{probe} = 435$, 445, 460, 470, 480, 500, 560, 600, 630, and 660 nm), and at the remaining probe wavelengths ($\lambda_{probe} = 425$, 530, 535 and 570 nm) a recovery of the bleaching signal ($\tau = 25(5)$ps) corresponding to the Soret and Q-bands was observed. These

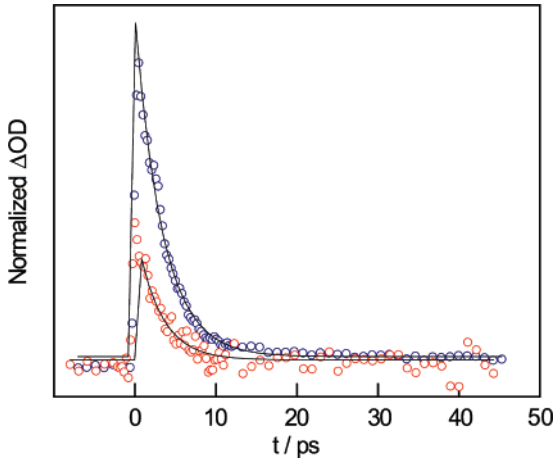

Figure 4. TA kinetics for dyad **2** in toluene with $\lambda_{exc} = 405$ nm and $\lambda_{probe} = 460$ nm (blue circles) and 660 nm (red circles). Monoexponential fits are also shown.

results simply reflect the quenching of the S_1 state with no observable intermediates.

TA experiments on **1** were also performed in a more polar solvent, THF ($\epsilon = 7.6$ as compared to $\epsilon = 2.4$ of toluene). The same transient results were observed in THF as were observed in toluene; namely, the TA spectrum was that of the S_1 excited state, which decayed with $\tau = 25$ ps.

A single phenylene spacer imposed between the two porphyrins reduces the center-to-center distance from $d_{D-A} = 17$ Å in dyad **1** to 13 Å in dyad **2**. The electronic absorption spectrum of dyad **2** is nearly identical to that of dyad **1**, and the spectral properties and thermodynamic driving forces (vide infra) for charge transfer are the same for both species. Figure 4 shows TA kinetics measured for dyad **2** in toluene with $\lambda_{probe} = 460$ and 660 nm. At both wavelengths, monoexponential decays with particularly fast time constants of $\tau \sim 4$ ps are observed. Clearly, the shortened bridge of dyad **2** results in accelerated S_1 quenching relative to dyad **1**. However, as was the case for dyad **1**, no spectral signature for PCET products is observed in dyad **2**. Additional visible wavelengths were also probed in dyad **2** ($\lambda_{probe} = 425-660$ nm). In all cases, a positive signal decaying on a commensurate time scale ($\tau = 6(3)$ ps) is observed, except in the Soret and Q-band regions where the recovery of a bleaching signal is observed on a corresponding time scale.

Having established the photophysics of dyads **1** and **2**, we turned our attention to the WF/SF mixed ligand adducts, employing 1-methylimidazole (1-MeIm) as the strong-field ligand. The first imperative was to verify that (HPX)Fe^{III} binds 1-MeIm only on the proximal side and leaves the distal Fe−OH unit intact to participate in PCET. Figure 5a shows the titration of 1-MeIm against (TMP)Fe^{III}−OH. This porphyrin lacks the Hangman pillar, but it is otherwise identical to (HPX)-Fe^{III}−OH. The spectral shifts are characterized by a sharpened, intensified, and red-shifted Soret band ($\lambda_{max} = 427$ nm) and sharpened and blue-shifted Q-bands ($\lambda_{max} = 534$, 565 nm), in addition to bleaching in the $\lambda = 450-500$-nm region. These features are characteristic of a low-spin (LS) bis-Im complex in which the OH^- has been displaced from the metal to produce a more symmetric coordination sphere.[39] Figure 5b and c show the spectral changes associated with addition of 1,5-dicyclohexylimidazole (dch-Im) and 1-methylimidazole (1-MeIm) to (HPX)Fe^{III}−OH in toluene over roughly the same concentration range. The bulkiness of dch-Im is sure to exclude it from binding on the same side as the Hangman group. In both 5b and 5c, the

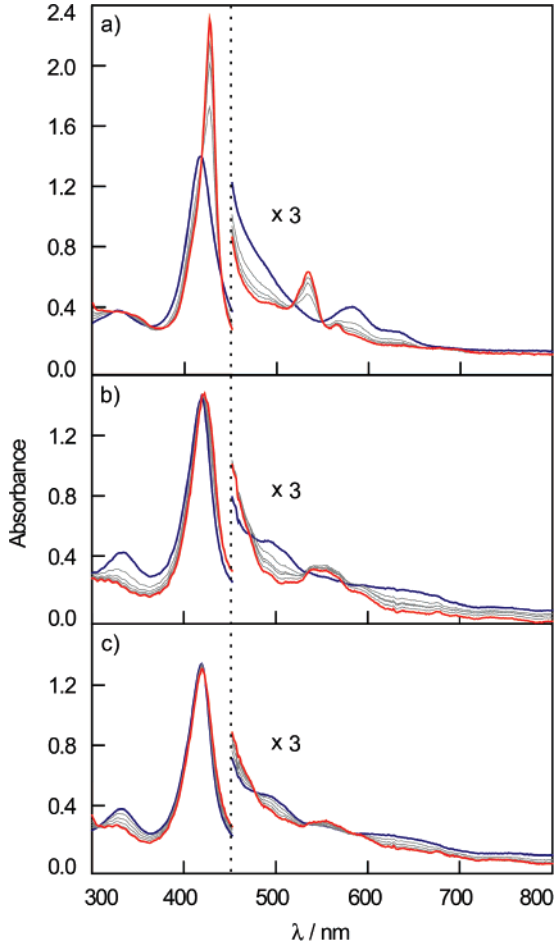

Figure 5. (a) Spectral evolution corresponding to titration of (a) 1-MeIm with (TMP)Fe^{III}−OH, (b) dch-Im with (HPX)Fe^{III}−OH, and (c) 1-MeIm with (HPX)Fe^{III}−OH. The initial spectrum (blue) was recorded in the absence of 1-MeIm, the final spectrum (red) contains 0.08 M 1-MeIm, and intermediate spectra (gray) are also shown.

spectral shifts are slight and not in accordance with a bis-Im adduct. Accordingly, we believe that the spectral changes in Figure 5b and c are associated with ligand binding to the heme on the proximal side of the porphyrin and an OH^- ligand on the Hangman side. Consistent with this assertion, computer models and the X-ray crystal analysis of the structure of (HPX)-Fe^{III}−OH[47] suggest that neither dch-Im nor 1-MeIm will fit inside the Hangman cavity. These results are consistent with NMR spectroscopy of PFe^{III}(X)(Im) species.[40]

The (E-P)Zn^{II} side of the dyad is also expected to bind one imidazole ligand to form a 5-coordinate species. Addition of 1-MeIm to a solution of (E-P)Zn^{II} results in spectral shifts consistent with imidazole binding; the Soret band shifted from $\lambda_{abs,max} = 405$ to 417 nm, and the Q-bands shifted from $\lambda_{abs,max} = 535$ and 571 nm to 547 and 580 nm, respectively. 1-MeIm reportedly binds axially to (TPP)Zn^{II} with a binding constant of $K \sim 5 \times 10^4$ M^{-1} in toluene.[83,84] A comparable axial binding constant for (E-P)Zn^{II} would require it to accept an axial 1-MeIm ligand at the concentrations required to bind to the Hangman porphyrin in the dyads. To ensure that the samples used for TA consisted of dyads in the same coordination state (one 1-MeIm bound to each of the two porphyrins), 1.0 M solutions of 1-MeIm were employed. Indeed, the electronic absorption spectrum of dyad **1** in toluene with 1.0 M 1-MeIm displays shifts in line with those of the constituent monomers ($\lambda_{abs,max}$(Soret) = 422 nm, $\lambda_{abs,max}$(Q) = 550 and 585 nm).

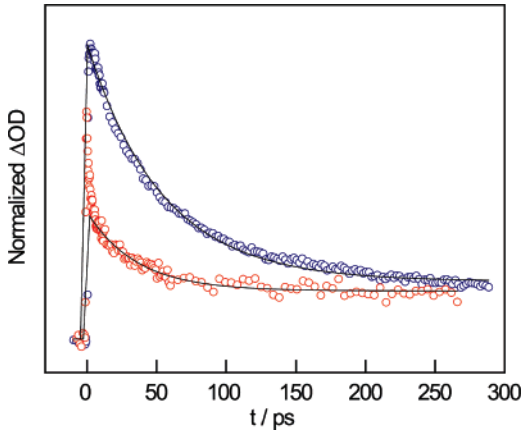

Figure 6. TA kinetics for dyad **1** in toluene with 1.0 M 1-MeIm, with $\lambda_{exc} = 405$ nm, and $\lambda_{probe} = 475$ nm (blue circles) and 675 nm (red circles).

Figure 6 shows TA kinetics measured for dyad **1** in a 1.0 M solution of 1-MeIm in toluene, with $\lambda_{probe} = 475$ and 675 nm. The $\lambda_{probe} = 475$-nm data exhibits a monoexponential decay ($\tau = 50(5)$ ps). The $\lambda_{probe} = 675$-nm signal also decays on a concomitant time scale ($\tau = 40(10)$ ps). Importantly, the absence of a rising signal associated with a (E-P$^{\bullet+}$)Zn^{II} species at this wavelength excludes the assignment of an S_1 excited state that reacts by charge transfer.

Discussion

PCET from the S_1 excited state of the (E-P)Zn^{II} component to the (HPX)Fe^{III}−OH is estimated to be thermodynamically favorable by $\Delta G^o \sim -0.8$ eV in dyad **1**. This estimate comes from

$$\Delta G^\circ = E_{1/2}(D^+/D) - E_{1/2}(A/A^-) - E_{0-0} + \Delta G(\epsilon) \quad (1)$$

where $E_{1/2}(D^+/D)$ is the ground state oxidation potential of the electron donor (taken as that of (octaethyl porphyrin)Zn^{II} ($E_{1/2}$-((OEP$^{\bullet+}$)Zn^{II}/(OEP)Zn^{II}) = +0.68 V vs Ag/AgCl),[85] $E_{1/2}$(A/A$^-$) is the ground state reduction potential of the electron acceptor (taken as that of $E_{1/2}$((TMP)Fe^{III}−OH/(TMP)Fe^{II}−OH$_2$) = −0.81 V vs Ag/AgCl),[86] E_{0-0} is the excited-state energy of the photoactive state of the electron donor or acceptor (2.17 eV for (E-P)Zn^{II} based on the spectral overlap of $Q_{0,0}$ absorption and emission bands), and $\Delta G(\epsilon)$ is a solvent-dependent Coulombic term that accounts for the spatial configuration of charges in a dielectric medium ($\Delta G(\epsilon) = 0.1$ V using the Born equation for a D−A distance of $d_{D-A} = 17$ Å, D/A radii of $r = 5$ Å, and in the solvent THF).

Despite the strongly favorable driving force available for photoinduced PCET in dyad **1**, TA spectroscopy experiments revealed no evidence of PCET intermediates. In particular, the $\lambda_{probe} = 650-700$-nm region was targeted to resolve the appearance of (P$^{\bullet+}$)Zn^{II}, with the assurance that no other potential transient species can contribute appreciably to the signal in this wavelength region; neither does the ground state have a significant optical density. Notwithstanding, the absence of a signal growth at this probe wavelength excludes PCET as a prevalent quenching mechanism of the S_1 excite state. The summary of the kinetics for dyads **1** and **2** is summarized in Table 1.

In the absence of PCET in **1**, the system was modified by shortening the electron tunneling distance by replacing the biphenylene spacer in dyad **1** with the phenylene spacer in dyad **2**. ET theory predicts an exponential distance dependence of

TABLE 1: Geometric and Kinetic Parameters for Hangman Bisporphyrins

dyad	r_{D-A}/Å	τ/ps	charge-transfer products observed?
1	17	25 ± 5	no
1 + 1MeIm	17	45 ± 10	no
2	13	6 ± 3	no

electron tunneling rates that arises from the overlap integral of the exponentially decaying wavefunction.[87,88] Compared with dyad **1** ($\tau = 25(5)$ ps), dyad **2** exhibits accelerated S_1 quenching ($\tau = 6(3)$ ps), but TA signals showing the presence of the charge-transfer product, (P$^{\bullet+}$)Zn^{II} are not observed; thus, ruling out the assignment of PCET in the more strongly coupled dyad **2**. Moreover, for either dyad, PCET is not observed in the more polar solvent, THF ($\epsilon = 7.6$). Charge-separation rates are known to be sensitive to the solvent dielectric constant, since it is a measure of how well the solvent environment is able to screen charge separation.[89] The invariance of S_1 quenching rates in both solvents for **1** and **2** provides further evidence that the S_1 excited state does not participate in charge separating reactions.

The heme center of the pentacoordinate (HPX)Fe^{III}OH Hangman is high spin (HS). We believe that a large degree of nuclear reorganization is demanded for PCET reactions involving the (HPX)Fe^{III}−OH center of dyads **1** and **2**. Figure 7 shows the energy-optimized geometries of the relevant subunit, PFe^{III}−OH, and its PCET product, PFe^{II}−OH$_2$, obtained from DFT electronic structure calculations. In addition to the bond-making and -breaking associated with the PT component of the reaction, the heme coordination sphere undergoes significant nuclear rearrangement upon reduction. In the case of PFe^{III}−OH, the symmetric distribution of the five d-electrons in HS Fe(III) favors a more spherical distribution of ligands, and hence, the coordination environment distorts from square−pyramidal geometry. The distortion of the Fe(III) ion is further induced by the presence of the axial and anionic OH$^-$ ligand. The Fe atom lies 0.538 Å out of the mean plane defined by the porphyrin N atoms, with average Fe−N bond lengths of 2.112 Å, and a shorter axial Fe−O bond (1.835 Å); these results are consistent with the crystal structure of Hangman porphyrins.[47] Conversely, the d^6 Fe(II) ion, which is the product of charge

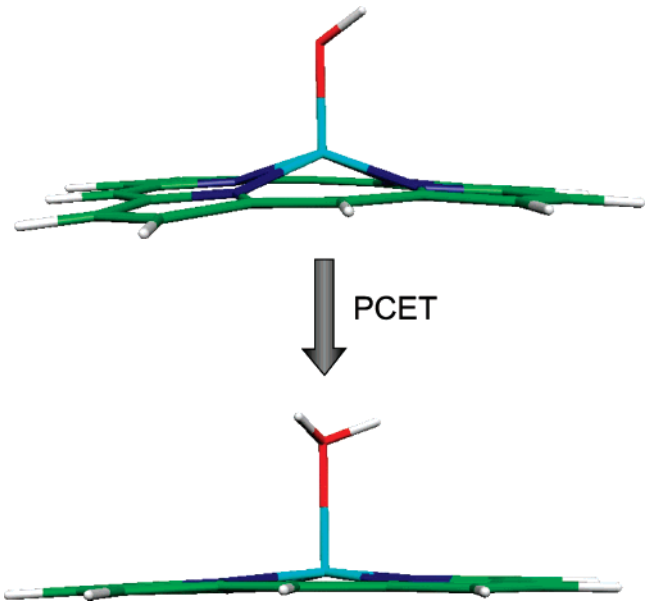

Figure 7. Energy-optimized geometries of PFe^{III}−OH (top, P = unsubstituted porphyrin) and PFe^{II}−OH$_2$ (bottom) from DFT calculations. The structural changes highlight the large degree of nuclear reorganization accompanying PCET at the Fe^{III}−OH center.

transfer, exhibits a relaxed preference for a spherical distribution of ligands, and the axial Fe−O bond is lengthened (to 2.229 Å). The confluence of these effects allows the Fe(II) atom to settle more deeply into the tetragonal pocket of the porphyrin; the Fe(II) atom is displaced from the porphyrin plane by only 0.190. The minimal electronic perturbation accompanying binding of 1-MeIm to Fe(III), as reflected in the modest spectral shifts (Figure 5c), suggests that the Fe(III) ion remains distorted and a large nuclear reorganization barrier likely persists for the reduction of (HPX)Fe^{III}−OH(1-MeIm) to (HPX)Fe^{II}−OH_2(1-MeIm). Along similar lines, facile ET in $PFe^{III}(Im)_2$−PZn^{II}(Im) dyads is ascribed to the location of the LS Fe(III) atom in the plane of the porphyrin, a configuration that is ideally poised for the production of Fe(II) with minimal nuclear rearrangement.[16]

In the absence of detectable PCET in dyads **1** and **2**, singlet EET and ISC can account for rapid S_1 quenching. Compared with other porphyrins, PFe^{III} species have a particularly large density of electronic states that can act as energy acceptors owing to the half-occupancy of the d-orbital manifold. A Förster resonant EET rate constant of $k_{EET} = 4.3 \times 10^9\ s^{-1}$ is calculated for **1** (see Supporting Information) on the basis of the absorption spectrum of (HPX)Fe^{III}−OH and the normalized emission spectrum of (E-P)Zn^{II} (Figure S1). The calculated Förster EET for dyad **1** in the presence of 1-MeIm is even slower ($k_{EET} = 3.5 \times 10^9\ s^{-1}$; see SI) owing to a pronounced red shift in the emission spectrum of (E-P)Zn^{II}(1-MeIm) ($\lambda_{em,max} = 584$ and 639 nm) combined with an attenuated fluorescence quantum yield and shorter unquenched lifetime. If Förster resonant EET were the only quenching mechanism, the lifetime ($1/\tau = 1/\tau_o + \tau_{EET}$) of the S_1 excited state for **1** would be expected to be $\tau \sim 200$ ps, considerably longer than the observed S_1 lifetime of $\tau = 25$ ps. The shorter donor−acceptor distance in **2** ($r = 13$ Å vs $r = 17$ Å for **1**) corresponds to a faster EET rate and shorter S_1 lifetime ($k_{EET} = 2.2 \times 10^{10}\ s^{-1}$, $\tau \sim 45$ ps). As for **1**, the Förster rate does not completely account for the observed quenching in **2** ($\tau_{obs} \sim 6$ ps). The disparity between observed quenching rates and those predicted by Förster resonance EET suggest a considerable contribution from Dexter energy transfer. With this mechanism, the double electron exchange employs the same orbital pathways that are required for charge transfer; consequently, both charge transfer and Dexter EET rates scale as an exponential decay with D−A distance, but the latter at twice the scaling constant.[90] The correspondence between charge transfer and Dexter EET has been demonstrated in bridged porphyrin dyad systems employing PZn^{II}s as donors and free-base porphyrins as acceptors.[68,91] EET rates through these systems, which have longer bridges (diarylethyne) than in **1** and **2**, approach $k_{EET} = 4 \times 10^{10}\ s^{-1}$, thus establishing the efficacy of Dexter EET.

In addition to EET dynamics, TA kinetics profiles suggest that early time dynamics has contributions of an accentuated ISC process. This is evident from the residual absorbance of singlet decay curves at a probe wavelength of ~460 nm (see Figures 2 and 4). The absorbance can plausibly be assigned the triplet (T_1) excited state of the (E-P)Zn^{II} component, formed as a result of efficient ISC. TA studies on the (E-P)Zn^{II} monomer show that the long-lived T_1 state (formed with a rate constant of $k_{ISC} \sim 5 \times 10^8\ s^{-1}$, and a quantum yield of $\Phi > 0.9$)[80] exhibits a molar extinction coefficient about 75%, as strong as the S_1 state in the 470-nm region, consistent with other reports.[16,17] If ISC operated at an unchanged rate in the dyads where competitive singlet quenching mechanisms are also operative, the T_1 yields corresponding to the observed S_1 lifetimes ($\Phi(T_1) = 1.3 \times 10^{-2}$ in dyad **1**, $\Phi(T_1) = 3.0 \times 10^{-3}$ in dyad **2**), would only contribute <1% of the initial S_1 intensity and would be lost in the baseline. However, the close proximity of a HS Fe(III) center in the dyads could accelerate ISC and boost the T_1 yields,[11,16−19] thus leaving a discernible long-lived signal. The relative signal observed at late times for dyad **1** ($\Delta OD_{470nm,300ps}/(\Delta OD_{470nm,2ps} = 0.10$) compared with unquenched (E-P)Zn^{II} ($\Delta OD_{470nm,10ns}/(\Delta OD_{470nm,2ps} = 0.70$) dictates that ISC could be accelerated by up to 10-fold in the dyad to account for the long-lived signal. Although insufficient to account for most of the observed quenching, the magnitude of the effect is in line with the measurements done by Albinsson and co-workers,[16] although those dyads exhibited longer lifetimes ($\tau = 119$−486 ps) due to the longer bridges separating the two porphyrin subunits.

In summary, the Hangman motif anchors an OH^- ligand in the distal position and directs a bulkier Im ligand to the proximal site of a heme, thus establishing a synthetically rare mixed WF/SF ligand set that includes the PCET substrate of OH^-. Transient spectroscopic experiments show that the HS PFe^{III}−OH, with or without a SF Im ligand, is not photoreduced by tethered Zn(II) porphyrins. Structural consideration of the iron coordination sphere of the HS PFe^{III}−OH center suggests PCET is unable to compete with EET and ISC, despite a strongly favorable driving force for the former, owing to the large nuclear reorganization associated with reduction, even in the absence of spin crossover. The results presented herein highlight the difficulty of orchestrating photoinduced PCET reactions at metallo-cofactors where the bonding-making and -breaking requirements of metal-centered PCET can impose sufficient impediments on charge transport that stereoelectronic factors of the heme become manifest. In view of these findings, the Hangman construct may be implemented for PCET investigations by (1) appending a photoexcitable donor in which EET is extremely slow or, alternatively, by (2) the use of a metal center that yield a LS complex for oxidized and reduced metal ion in a WF/SF ligand field. These investigations are currently underway.

Acknowledgment. We thank Dr. Christopher Chang for synthesis of Hangman monomer (HPX)Fe^{III}−OH and Joel Rosenthal for the synthesis of **8**. Financial support for this research was provided by the Department of Energy (DOE DEFG02-05ER15745) and the National Institutes of Health.

Supporting Information Available: Förster energy transfer rate calculations for the bisporphyrin dyads with pertinent absorption and emission spectra. This material is available free of charge via the Internet at http://pubs.acs.org.

References and Notes

(1) Kalyanasundaram, K. *Photochemistry of Polypyridine and Porphyrin Complexes*; Academic Press: San Diego, 1992; Chapter 15, pp 487−556.

(2) Liang, Z.-X.; Nocek, J. M.; Huang, K.; Hayes, R. T.; Kurnikov, I. V.; Beratan, D. N.; Hoffman, B. M. *J. Am. Chem. Soc.* **2002**, *124*, 6849−6859.

(3) Crnogorac, M. M.; Kostic, N. M. *Inorg. Chem.* **2000**, *39*, 5028−5035.

(4) Furukawa, Y.; Ishimori, K.; Morishima, I. *Biochemistry* **2000**, *39*, 10996−11004.

(5) Tollin, G. In *Electron Transfer in Chemistry*; Balzani, V., Ed; Wiley: Weinheim, 2001; Vol. IV, pp 202−231.

(6) Nocek, J. M.; Zhou, J. S.; De Forest, S.; Priyadarshy, S.; Beratan, D. N.; Onuchic, J. N.; Hoffman, B. M. *Chem. Rev.* **1996**, *96*, 2459−2490.

(7) McLendon, G. L.; Winkler, J. R.; Nocera, D. G.; Mauk, M. R.; Mauk, A. G.; Gray, H. B. *J. Am. Chem. Soc.* **1985**, *107*, 739−740.
(8) de Rege, P. J. F.; Williams, S. A.; Therien, M. J.; *Science* **1995**, *269*, 1409−1413.
(9) Osuka, A.; Maruyama, K.; Mataga, N.; Asahi, T.; Yamazaki, I.; Tamai, N. *J. Am. Chem. Soc.* **1990**, *112*, 4958−4959.
(10) Osuka, A.; Tanabe, N.; Kawabata, S.; Yamazaki, I.; Nishimura, Y. *J. Org. Chem.* **1995**, *60*, 7177−7185.
(11) Brookfield, R. L.; Ellul, H.; Harriman, A. *J. Chem. Soc. Faraday Trans. 2* **1985**, *81*, 1837−1848.
(12) Mataga, N.; Yao, H.; Okada, T.; Kanda, Y.; Harriman, A. *Chem. Phys.* **1989**, *131*, 473−480.
(13) Portela, C. F.; Brunckova, J.; Richards, J. L.; Schöllhorn, B.; Iamamoto, Y.; Magde, D.; Traylor, T. G.; Perrin, C. L. *J. Phys. Chem. A* **1999**, *103*, 10540−10552.
(14) Helms, A.; Heiler, D.; McLendon, G. *J. Am. Chem. Soc.* **1992**, *114*, 6227−6238.
(15) Helms, A.; Heiler, D.; McLendon, G. *J. Am. Chem. Soc.* **1991**, *113*, 4325−4327.
(16) Pettersson, K.; Kilså, K.; Mårtensson, J.; Albinsson, B. *J. Am. Chem. Soc.* **2004**, *126*, 6710−6719.
(17) Kilså, K.; Kajanus, J.; Larsson, S.; Macpherson, A. N.; Mårtensson, J.; Albinsson, B. *Chem.—Eur. J.* **2001**, *7*, 2122−2133.
(18) Asano-Someda, M.; Kaizu, Y. *Inorg. Chem.* **1999**, *38*, 2303−2311.
(19) Toyama, N.; Asano-Someda, M.; Ichino, T.; Kaizu, Y. *J. Phys. Chem. A* **2000**, *104*, 4857−4865.
(20) Denisov, I. G.; Makris, T. M.; Sligar, S. G.; Schlichting, I. *Chem. Rev.* **2005**, *105*, 2253−2278.
(21) Sono, M.; Roach, M. P.; Coulter, E. D.; Dawson, J. H. *Chem. Rev.* **1996**, *96*, 2841−2887.
(22) Dunford, H. B. *Heme Peroxidases*; Wiley: New York, 1999.
(23) Watanabe, Y. In *The Porphyrin Handbook*; Kadish, K. M.; Smith, K. M.; Guilard, R., Eds.; Academic Press: San Diego, 2000; Vol. 4, pp 97−117.
(24) Newcomb, M.; Zhang, R.; Chandrasena, R. E. P.; Halgrimson, J. A.; Horner, J. H.; Makris, T. M.; Sligar, S. G. *J. Am. Chem. Soc.* **2006**, *128*, 4580−4581.
(25) Hiner, A. N. P.; Raven, E. L.; Thorneley, R. N. F.; Garcia-Canovas, F.; Rodriguez-Lopez, J. N. *J. Inorg. Biochem.* **2002**, *91*, 27−34.
(26) Ozaki, S.-I.; Roach, M. P.; Matsui, T.; Watanabe, Y. *Acc. Chem. Res.* **2001**, *34*, 818−825.
(27) Poulos, T. L.; Kraut, J. *J. Biol. Chem.* **1980**, *255*, 8199−8205.
(28) Matsui, T.; Ozaki, S-I.; Liong, E.; Phillips, G. N.; Watanabe, Y. *J. Biol. Chem.* **1999**, *274*, 2838−2844.
(29) Derat, E.; Shaik, S. *J. Phys. Chem. B* **2006**, *110*, 10526−10533.
(30) Low, D. W.; Winkler, J. R.; Gray, H. B. *J. Am. Chem. Soc.* **1996**, *118*, 117−120.
(31) Berglund, J.; Pascher, T.; Winkler, J. R.; Gray, H. B. *J. Am. Chem. Soc.* **1997**, *119*, 2464−2469.
(32) Poulos, T. L.; Finzel, B. C.; Howard, A. J. *Biochemistry* **1986**, *25*, 5314−5322.
(33) Meunier, B.; de Visser, S. P.; Shaik, S. *Chem. Rev.* **2004**, *104*, 3947−3980.
(34) Hoganson, C. W.; Pressler, M. A.; Proshlyakof, D. A.; Babcock, G. T. *Biochim. Biophys. Acta* **1998**, *1365*, 170−174.
(35) Ferguson-Miller, S.; Babcock, G. T. *Chem. Rev.* **1996**, *96*, 2889−2907.
(36) Reece, S. Y.; Hodgkiss, J. M.; Stubbe, J.; Nocera, D. G. *Philos. Trans. R. Soc. London, Ser. B* **2006**, *361*, 1351−1364.
(37) Hodgkiss, J. M; Rosenthal, J; Nocera, D. G. In *Handbook of Hydrogen Transfer*; Hynes, J. T., Klinman, J. P., Limbach, H.-H., Schowen, R. L., Eds; Wiley-VCH: Weinheim, Germany, 2006; Vol. II, Part IV, Chapter 17, pp 503−562.
(38) Collins, D. M.; Countryman, R.; Hoard, J. L. *J. Am. Chem. Soc.* **1972**, *94*, 2066−2072.
(39) Walker, F. A.; Lo, M.-W.; Ree, M. T. *J. Am. Chem. Soc.* **1976**, *98*, 5552−5559.
(40) Goff, H. *J. Am. Chem. Soc.* **1980**, *102*, 3252−3254.
(41) Dawson, J. H. *Science* **1988**, *240*, 433−439.
(42) Sono, M.; Roach, M. P.; Coulter, E. D.; Dawson, J. H. *Chem. Rev.* **1996**, *96*, 2841−2887.
(43) Ozaki, S.; Roach, M. P.; Matsui, T.; Watanabe, Y. *Acc. Chem. Res.* **2001**, *34*, 818−825.
(44) Poulos, T. L. *Adv. Inorg. Biochem.* **1988**, *7*, 1−36.
(45) Chang, C. J.; Chng, L. L.; Nocera, D. G. *J. Am. Chem. Soc.* **2003**, *125*, 1866−1876.
(46) Chng, L. L.; Chang, C. J.; Nocera, D. G. *Org. Lett.* **2003**, *5*, 2421−2424.
(47) Yeh, C. Y.; Chang, C. J.; Nocera, D. G. *J. Am. Chem. Soc.* **2001**, *123*, 1513−1514.
(48) Dempsey, J. L.; Esswein, A. J.; Manke, D. R.; Rosenthal, J.; Soper, J. D.; Nocera, D. G. *Inorg. Chem.* **2005**, *44*, 6879−6892.
(49) Armarego, W. L. F.; Perrin, D. D. *Purification of Laboratory Chemicals*, 4th Ed.; Butterworth-Heinmann: Oxford, 1996.
(50) Yu, L.; Muthukumaran, K.; Sazanovich, I. V.; Kirmaier, C.; Hindin, E.; Diers, J. R.; Boyle, P. D.; Bocian, D. F.; Holten, D.; Lindsey, J. S. *Inorg. Chem.* **2003**, *42*, 6629−6647.
(51) Buchler, J. W. In *The Porphyrins*; Dolphin, D., Ed.; Academic Press: New York, 1978; Vol. 1, Part A.
(52) Chang, C. J.; Yeh, C.-Y.; Nocera, D. G. *J. Org. Chem.* **2002**, *67*, 1403−1406.
(53) Zhu, L.; Duquette, J.; Zhang, M. *J. Org. Chem.* **2003**, *68*, 3729−3732.
(54) Hombrecher, H. K.; Horter, G. *Liebigs Ann. Chem.* **1991**, 219−227.
(55) Ishiyama, T.; Murata, M.; Miyaura, N. *J. Org. Chem.* **1995**, *60*, 7508−7510.
(56) Chang, C. J.; Loh, Z.-H.; Deng, Y.; Nocera, D. G. *Inorg. Chem.* **2003**, *42*, 8262−8269.
(57) Hodgkiss, J. M.; Chang, C. J.; Pistorio, B. J.; Nocera, D. G. *Inorg. Chem.* **2003**, *42*, 8270−8277.
(58) Damrauer, N. H.; Hodgkiss, J. M.; Rosenthal, J.; Nocera, D. G. *J. Phys. Chem. B* **2004**, *108*, 6315−6321.
(59) Loh, Z.-H.; Miller, S. E.; Chang, C. J.; Carpenter, S. D.; Nocera, D. G. *J. Phys. Chem. A* **2002**, *106*, 11700−11708.
(60) te Velde, G.; Bickelhaupt, F. M.; van Gisbergen, S. J. A.; Fonseca, Guerra, C.; Baerends, E. J.; Snijders, J. G.; Ziegler, T. *J. Comput. Chem.* **2001**, *22*, 931−967.
(61) Fonseca Guerra, C.; Snijders, J. G.; te Velde, G.; Baerends, E. J. *Theor. Chem. Acc.* **1998**, *99*, 391−403.
(62) Becke, A. D. *Phys. Rev. A: At., Mol., Opt. Phys.* **1988**, *38*, 3098−3100.
(63) Perdew, J. P.; Chevary, J. A.; Vosko, S. H.; Jackson, K. A.; Pederson, M. R.; Singh, D. J.; Fiolhais, C. *Phys. Rev. B: Condens. Matter Mater. Phys.* **1992**, *46*, 6671−6687.
(64) Felton, R. H. In *The Porphyrins*; Dolphin, D., Ed.; Academic Press: New York, 1978; Vol. V, pp 53−126.
(65) Fajer, J.; Borg, D. C.; Forman, A.; Dolphin, D.; Felton, R. H. *J. Am. Chem. Soc.* **1970**, *92*, 3451−3459.
(66) Chosrowjan, H.; Tanigichi, S.; Okada, T.; Takagi, S.; Arai, T.; Tokumam, K. *Chem. Phys. Lett.* **1995**, *242*, 644−649.
(67) Imahori, H.; Hagiwara, K.; Aoki, M.; Akiyama, T.; Taniguchi, S.; Okada, T.; Shirakawa, M.; Sakata. Y. *J. Am. Chem. Soc.* **1996**, *118*, 11771−11782.
(68) Yang, S. I.; Seth, J.; Balasubramanian, T.; Kim, D.; Lindsey, J. S.; Holten, D.; Bocian, D. F. *J. Am. Chem. Soc.* **1999**, *121*, 4008−4018.
(69) Kilså, K.; Macpherson, A. N.; Gillbro, T.; Mårtensson, J.; Albinsson, B. *Spectrochim. Acta, Part A* **2001**, *57*, 2213−2227.
(70) Yu, L.; Lindsey, J. S. *Tetrahedron* **2001**, *57*, 9285−9298.
(71) Gouterman, M. In *The Porphyrins*; Dolphin, D., Ed.; Academic Press: New York, 1978; Vol. 3−5.
(72) Kasha, M.; Rawls, H. R.; El-Bayoumi, M. A. *Pure Appl. Chem.* **1965**, *11*, 371−392.
(73) Andersson, M.; Davidsson, J.; Korppi-Tommola, J.; Peltola, T.; Hammarström, L. *J. Phys. Chem. B.* **1999**, *103*, 3258−3262.
(74) Liu, X.; Yeow, E. K. L.; Velate, S.; Steer, R. P. *Phys. Chem. Chem. Phys.* **2006**, *8*, 1298−1309.
(75) Huppert, D.; Straub, K. D.; Rentzepis, P. M. *Proc. Natl. Acad. Sci. U.S.A.* **1977**, *74*, 4139−4143.
(76) Tait, C. D.; Holten, D.; Gouterman, M. *Chem. Phys. Lett.* **1983**, *100*, 268−272.
(77) Liang, Y.; Negus, D. K.; Hochstrasser, R. M.; Gunner, M.; Dutton, P. L. *Chem. Phys. Lett.* **1981**, *84*, 236−240.
(78) Dixon, D. W.; Kirmaier, C.; Holten, D. *J. Am. Chem. Soc.* **1985**, *107*, 808−813.
(79) Ohno, O.; Kaizu, Y.; Kobayashi, H. *J. Chem. Phys.* **1985**, *82*, 1779−1787.
(80) Gradyushko, A. T.; Tsvirko, M. P. *Opt. Spect.* **1971**, *31*, 291−295.
(81) Collman, J. P.; Brauman, J. I.; Doxsee, K. M.; Halbert, T. R.; Bunnenberg, E.; Linder, R. E.; LaMar, G. N.; Gaudio, J. D.; Lang, G.; Spartalian, K. *J. Am. Chem. Soc.* **1980**, *102*, 4182−4192.
(82) Soper, J. D.; Kryatov, S. V.; Rybak-Akimova, E.V.; Nocera, D. G. *J. Am. Chem. Soc.* **2007**, *129*, 5069−5075.
(83) Brewer, C. T.; Brewer, G. *J. Chem. Soc. Dalton Trans.* **1990**, 843−847.
(84) Marbury, G. S.; Brewer, C.; Brewer, G. *J. Chem. Soc. Dalton Trans.* **1991**, 1377−1378.
(85) Chang, C. K.; Fajer, J. *J. Am. Chem. Soc.* **1980**, *102*, 848−851.
(86) Swistak, C.; Mu, X. H.; Kadish, K. M. *Inorg. Chem.* **1987**, *26*, 4360−4366.

(87) Hopfield, J. J. *Proc. Natl. Acad. Sci. U.S.A.* **1974**, *71*, 3640−3644.
(88) Closs, G. L.; Miller, J. R. *Science* **1988**, *240*, 440−447.
(89) *Techniques of Chemistry*, 3rd ed.; Vol. II, Organic Solvents: Physical Properties and Methods of Purification; p 57.
(90) Closs, G. L.; Johnson, M. D.; Miller, J. R.; Piotrowiak, P. *J. Am. Chem. Soc.* **1989**, *111*, 3751−3753.
(91) Strachan, J.-P.; Gentemann, S.; Seth, Y.; Kalsbeck, W. A.; Lindsey, J. S.; Holten, D.; Bocian, D. F. *J. Am. Chem. Soc.* **1997**, *119*, 11191−11201.